11-26-2006

Multiwalled ice helixes and ice nanotubes

Jaeil Bai
University of Nebraska-Lincoln, jbai2@unl.edu

Jun Wang
University of Nebraska-Lincoln, jwang3@unl.edu

Xiao Cheng Zeng
University of Nebraska-Lincoln, xzeng1@unl.edu

Published in *Proceedings of the National Academy of Sciences of the United States,* vol. 103, no. 52 (December 26, 2006), pp. 19664-19667. Published online December 14, 2006. http://www.pnas.org/cgi/doi/10.1073/pnas.0608401104

Multiwalled ice helixes and ice nanotubes

Jaeil Bai, Jun Wang, and X. C. Zeng*

Department of Chemistry and Nebraska Center for Materials and Nanoscience, University of Nebraska, Lincoln, NE 68588

Edited by Benjamin Widom, Cornell University, Ithaca, NY, and approved October 31, 2006 (submitted September 2006)

Abstract – We report six phases of high-density nano-ice predicted to form within carbon nanotubes (CNTs) at high pressure. High-density nano-ice self-assembled within smaller-diameter CNT (17,0) exhibits a double-walled helical structure where the outer wall consists of four double-stranded helixes, which resemble a DNA double helix, and the inner wall is a quadruple-stranded helix. Four other double-walled nano-ices, self-assembled respectively in two larger-diameter CNTs (20,0 and 22,0), display tubular structure. Within CNT (24,0), the confined water can freeze spontaneously into a triple-walled helical nano-ice where the outer wall is an 18-stranded helix and the middle and inner walls are hextuple-stranded helixes.

Keywords – carbon nanotube, high density nano-ice, nano-ice helix

Bulk ice is known to have 15 crystalline phases (1, 2). Among them, 12 phases are only stable (or metastable) under high pressures; for example, the ice II phase formed in the core of the moon Ganymede of Jupiter and the moon Titan of Saturn (3). In contrast, in microscopic confinement such as nanochannels, water can freeze into nano-ices that show rich structures (phases) as well (4–14). Indeed, when liquid water is encapsulated in nanochannels such as carbon nanotubes (CNTs) (15), water molecules can align into certain quasi-one-dimensional structures (16–25) due to the interplay between nanoscale confinement and strong intermolecular hydrogen bonding. Hence, encapsulation of water in CNTs offers an opportunity to explore dimensionally confined fluid dynamics (nanofluidics) (22) and phase transitions [e.g., filling-emptying (16–18, 24) and freezing (4–14)]. In the case of the freezing transition for bulk water, the stable (or metastable) ice structure selected is highly sensitive to external controlling parameters, such as pressure and temperature (26). However, in microscopic confinement, an additional external parameter, the scale of confinement (e.g., diameter of CNTs), might lead to even richer ice structures (phases) not found in the bulk. To date, five low-density nano-ices have been detected via x-ray diffraction (7, 13), NMR (11), and vibrational spectroscopy (14); none bear structural similarity to known bulk ices. These five low-density nano-ice phases all exhibit single-walled tubular morphologies, including the pentagon ice nanotube (INT) (provisionally named nano-ice I), hexagon INT (nano-ice II), heptagon INT (nano-ice III), octagon INT (nano-ice IV), and nonagon INT (nano-ice V). Additionally, a more complex nano-ice structure, the core/sheath nano-ice, was recently revealed via neutron scattering measurement (12) where the core is a single-profile water chain and the sheath is just an octagon INT (tentatively named nano-ice IVa). Note that these single-walled INTs are all formed under atmospheric pressure.

When bulk ice is compressed at high pressures, the hydrogen bond framework can undergo a sequence of distortion, breakage, and reformation, which may lead to new high-density ices. Similarly, we expect that new structures of high-density nano-ices may form within CNTs when high pressure is applied along the axial direction. To test this possibility, we carried out a series of four molecular dynamics (MD) simulations to explore formation of high-density nano-ices in four prototype zigzag CNTs described by the chiral vector (17,0), (20,0), (22,0), and (24,0). Note that the zigzag CNT can be viewed as rolling up a graphene sheet into a cylinder along a "zigzag" line direction (namely, the direction perpendicular to a carbon–carbon bond in the graphene plane). The diameter of the four CNTs ranges from 1.35 to 1.90 nm.

Results and Discussion

In the first series of MD simulations, liquid water was initially confined to the (17,0) CNT at low pressure (P_{zz} = 1 MPa) and high temperature (320 K). In the ensuing simulation, the temperature was lowered stepwise from 320 to 290 K to 270 to 240 K. At each temperature, 5-to 20-ns simulations were carried out, respectively. At the lowest temperature (240 K), the confined water was observed to spontaneously freeze into a heptagon INT (i.e., nano-ice III) after 16 ns of equilibration. Next, with the temperature controlled at 250 K, we increased the axial pressure instantly in four steps: (*i*) P_{zz} = 1 GPa, (*ii*) P_{zz} = 2 GPa, (*iii*) P_{zz} = 3 GPa, and (*iv*) P_{zz} = 4 GPa. At P_{zz} = 1 GPa, we observed that the heptagon INT was transformed into a higher-density nano-ice: the core/sheath nano-ice (i.e., from nano-ice III to nano-ice IVa). At P_{zz} = 2 and 3 GPa, no solid-to-solid phase transition was observed after a 20-ns simulation. However, at P_{zz} = 4 GPa, we observed that the nano-ice IVa was transformed into a double-walled helical nano-ice (Fig. 1a and b). Unlike the single-walled nano-ice morphologies (i.e., nano-ice I–V), whose hydrogen-bond networks can be viewed as stacked-water polygons, the helical nano-ice consists of two walls: The outer wall can be viewed as either an octuple-stranded helix (Fig. 1c) or a braid of four double helixes, whereas the inner wall is a quadruple-stranded helix (Fig. 1d). Interestingly, the water double helix resembles the DNA double helix (27) in structure and in intrahelix hydrogen-bonding interaction.

At the ultra-high axial pressure (4 GPa), we observed that many hydrogen bonds of the lower-density nano-ice IVa were broken at the early stage of simulation. After the simulated passage of a few tens of nanoseconds, rearrangement of the water molecules eventually led the helical nano-ice structure. Like low-density nano-ice I–V, the high-density helical nano-ice satisfies the bulk ice rule with every water molecule hydrogen-bonded to exactly four nearest-neighbor water molecules (28). Specifically, every water molecule in the outer wall is hydrogen-bonded to three nearest-neighbors in the double helix (highlighted in gold in Fig. 1*c*) and to one (the fourth nearest neighbor) in the inner wall. Conversely, every molecule of the inner wall is only hydrogen-bonded to two nearest neighbors within the quadruple helix; the other two hydrogen bonds are to nearest neighbors in the outer wall. In this way, the four pairs of the double helix (in the outer wall) are in registry with the quadruple helix (in the inner wall), fulfilling the bulk ice rule.

The second series of MD simulations involved a CNT (20,0) with a slightly larger diameter of 1.585 nm. After the confined liquid water reached equilibrium at 250 K and 1 MPa, the pressure was increased instantly in three steps: (*i*) P_{zz} = 500 MPa, (*ii*)

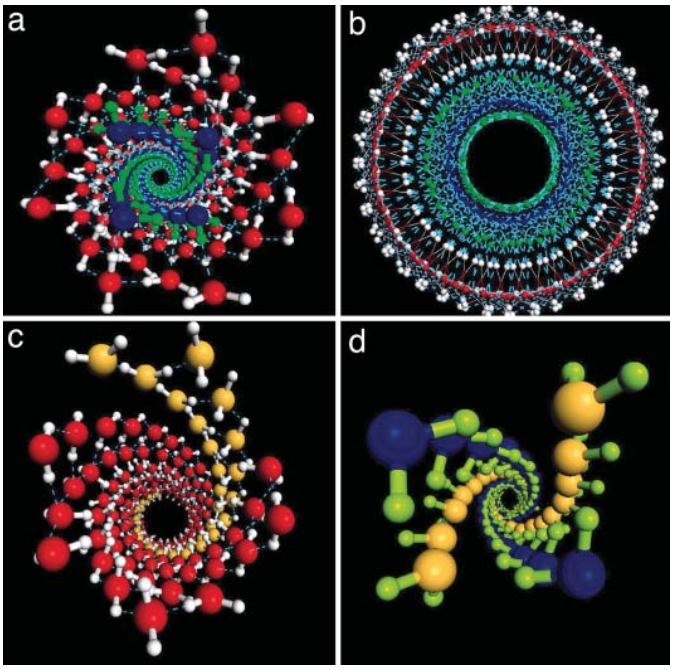

Fig. 1. Snapshots of quenched molecular coordinates of the helical nano-ice formed in (17,0) CNT at 4 GPa axial pressure. (*a*) Top view of the double-walled nano-ice helix in the axial direction. Water molecules in the outer wall are in red–white, whereas those in the inner wall are in blue–green (the blue dashed lines denote hydrogen bonds). (*b*) Projected top view in the axial direction. Due to the helicity, the projected top view shows ring-like outer and inner wall structures. (*c*) The outer wall: an octuple-stranded helix consisting of four double helixes (one of the four is highlighted by gold). (*d*) The inner wall: a quadruple-stranded helix where two strands (gold) are proton donors and two (blue) are proton acceptors to molecules of the outer wall.

P_{zz} = 2 GPa, and (*iii*) P_{zz} = 3 GPa. At P_{zz} = 500 MPa, we observed that the liquid water froze spontaneously into a new high-density nano-ice with a double-walled tubular structure (Fig. 2*a*–*c*). The outer wall is a staggered-octagon nanotube, whereas the inner wall is a staggered tetragon. The INT also contains core water molecules with two molecules per unit cell (Fig. 2*d*). Note that a stand-alone octagon or tetragon INT can satisfy the ice rule by itself. However, because of the existence of the core water molecules, both the outer and inner INTs adopt the staggered structures to fulfill the ice rule.

Increasing the pressure to 2 GPa results in a solid-to-solid transition. Again, the new high-density nano-ice has a double-walled tubular structure where the outer wall is a hendecagon nanotube, and the inner wall is a pentagon nanotube (Fig. 2*e* and *f*). No core water molecules are present. Lastly, at the highest pressure simulated (3 GPa), another solid-to-solid phase transition was observed. The hendecagon/pentagon nano-ice transformed into a new high-density double-walled nano-ice containing core water molecules (Fig. 2*g*). Here, the outer wall is a weakly helical hendecagon nanotube, whereas the inner wall is transformed from a pentagon to a weakly helical hexagon nanotube. The core is a single-profile water chain. The greatly increased density can be seen from the projected top view of the two nano-ices (Fig. 2*f* and *h*).

The third series of MD simulations involved another CNT (22,0) with diameter 1.74 nm. After the confined liquid water reached equilibrium at 250 K and 1 MPa, the pressure was instantly raised to 800 MPa. Again, the liquid froze spontaneously into a high-density double-walled tubular structure containing core molecules (Fig. 3*a*). Here, the outer wall is a decagon-like

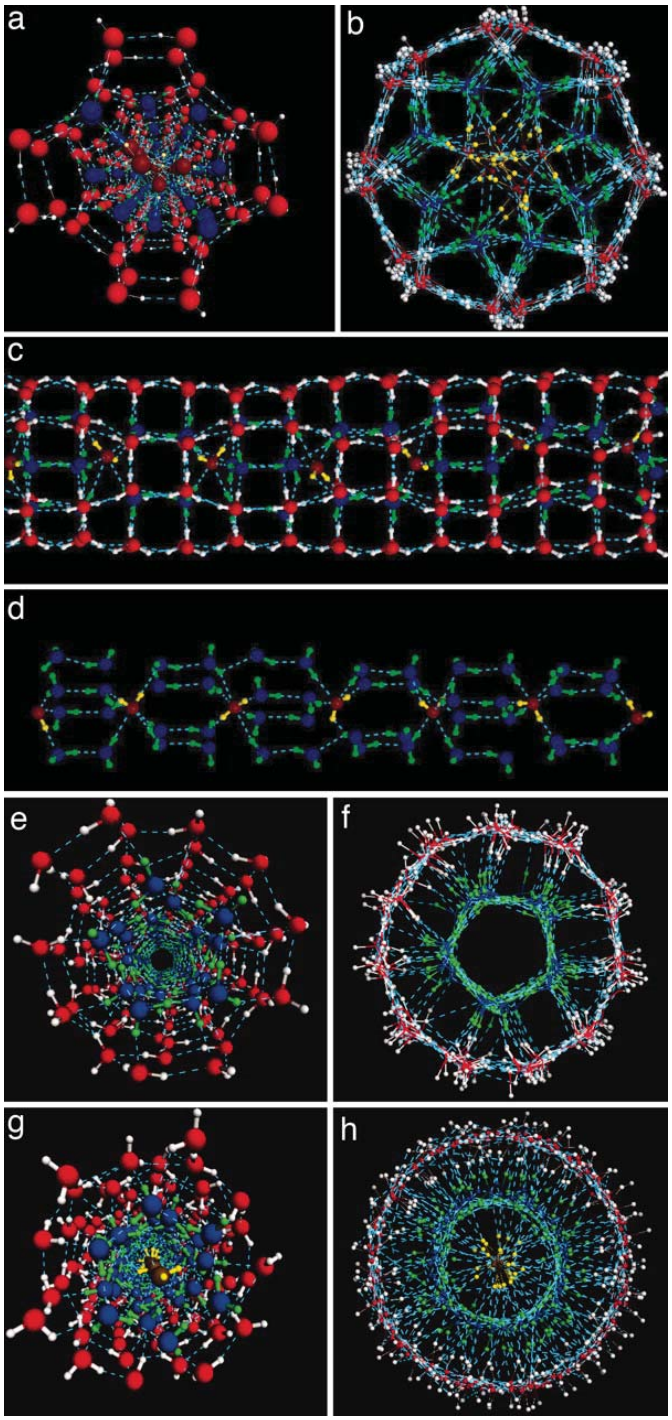

Fig. 2. Snapshots of quenched molecular coordinates of nano-ices formed in (20,0) CNT at 500 MPa (*a*–*d*), 2 GPa (*e* and *f*), and 3 GPa (*g* and *h*) axial pressure. Components of the outer wall are in red–white, those of the inner wall are in blue–green, and core water molecules are in maroon–yellow. (*a* and *b*) Top (*a*) and projected top (*b*) view of the double-walled tubular nano-ice in the axial direction; the outer wall is a staggered-octagon nanotube, whereas the inner wall is a staggered-tetragon nanotube. (*c* and *d*) Side view of the nano-ice (*c*) and inner wall (*d*). Each unit cell of the nanotube contains two core water molecules. (*e* and *f*) Top (*e*) and projected top (*f*) view of the double-walled tubular nano-ice in the axial direction; the outer wall is a hendecagon nanotube, and the inner wall is a pentagon nanotube. (*g* and *h*) Top (*g*) and projected top (*h*) view of the double-walled tubular nano-ice containing core water molecules; the outer wall is a weakly helical hendecagon nanotube; the inner wall is a weakly helical hexagon nanotube. Due to the helicity, the projected top view shows ring-like outer and inner wall structures.

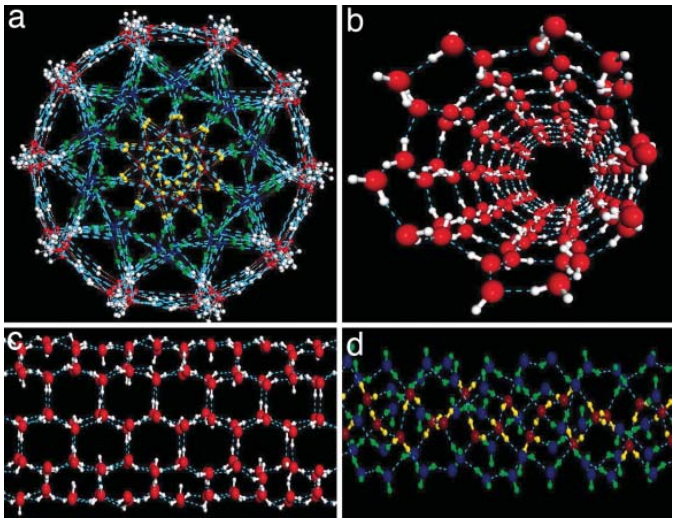

Fig. 3. Snapshots of quenched molecular coordinates of the nano-ice formed in (22,0) CNT at 800 MPa axial pressure. (*a*) Projected top view of the double-walled nano-ice in the axial direction. (*b* and *c*) Top (*b*) and side (*c*) view of the outer wall, which is the (5,5) armchair ice nanotube. (*d*) Side view of the inner wall and core water molecules (maroon–yellow). The inner wall is a staggered-pentagon nanotube.

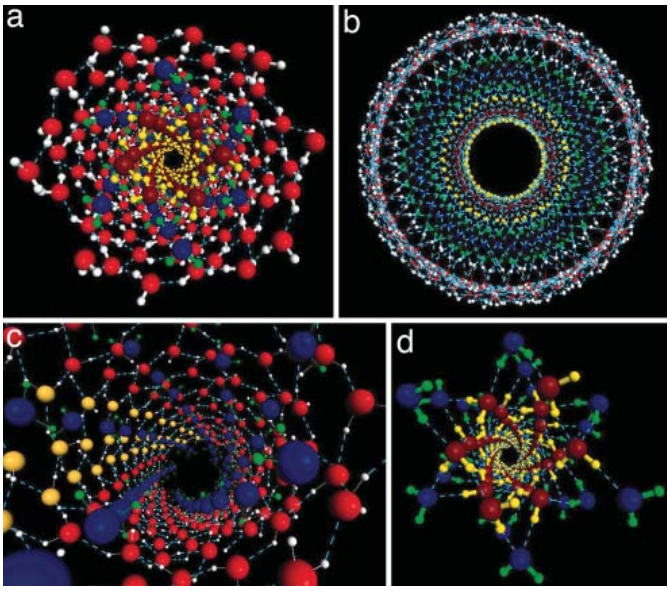

Fig. 4. Snapshots of quenched molecular coordinates of the triple-walled nano-ice formed in (24,0) CNT at 800 MPa axial pressure. Components of the outer wall are in red–white, those of the middle wall are in blue–green, and those of inner wall are in maroon–yellow. (*a* and *b*) Top (*a*) and projected top (*b*) view of the triple-walled nano-ice helix in the axial direction. The outer wall is an 18-stranded helical nanotube; the middle and inner walls are hextuple-stranded helixes. (*c*) Top view of the outer wall and the middle wall. The outer wall can be viewed as a network of interlinked hexagons and tetragons. Every strand in the middle wall is in registry with three strands (gold colored) in the outer wall. (*d*) Top view of the middle and inner wall.

nanotube (Fig. 3*b*) with a structure similar to that of (5,5) armchair CNT (Fig. 3*c*), whereas the inner wall is a staggered pentagon nanotube (Fig. 3*d*). The core is a single-stranded water helix (Fig. 3*d*). Because the diameter of the (22,0) CNT is larger, it is expected that more complex nano-ice structures can be self-assembled under high pressures. Indeed, component of three water morphologies, the (5,5) armchair, the staggered pentagon, and the single-profile helix, is another remarkable way for the water molecules to arrange themselves and to fulfill the ice rule. The formation of an armchair water tube is particularly noteworthy. It is known that the armchair tube can be viewed as rolling up a graphene sheet along a carbon–carbon bond direction. Such a graphene-sheet like water structure has been reported previously in the formation of a two-dimensional bilayer ice within a hydrophobic slit pore (29). Therefore, the armchair water tube can be viewed as rolling up one sheet of two-dimensional bilayer ice.

Finally, the fourth series of MD simulations involved a CNT (24,0) with the largest diameter (1.90 nm) considered in this study. After the confined liquid water reached equilibrium at 250 K and 1 MPa, the pressure was raised instantly to 800 MPa. In stark contrast to the previous cases, the confined liquid froze spontaneously into a high-density triple-walled helical structure (Fig. 4*a* and *b*). Here, the outer wall is an 18-stranded helical nanotube (Fig. 4*c*), whereas both the middle and inner walls are hextuple-stranded helixes (Fig. 4 *c* and *d*). It appears that the diameter of the (24,0) CNT is large enough to host a triple-walled nano-ice helix. Interestingly, the middle wall only serves as a hydrogen-bonding "bridge" to connect the outer wall and inner wall; water molecules in the middle wall (in blue–green) do not have any hydrogen-bonding neighbors within the middle wall itself.

In summary, we have demonstrated, using MD simulation, previously unknown double- and triple-walled nano-ice morphologies within CNTs. Unique to the freezing of water in nanoconfinement is the extra controlling parameter, the scale of the confinement, in addition to the temperature and pressure. This additional parameter may lead to much richer and amorphous ice morphologies than found in the bulk. The water double helix in the nano-ice shows structural similarity to the DNA double helix. In the CNT (22,0), an armchair (5,5) INT emerges, marking the onset of graphene-like nano-ice in the CNT. In closing, the richness of the bulk and nano-ice phases are a testament to the adaptability and versatility of the water–hydrogen bond framework to a change of external environment, either on the outer planets or within microscopic nanochannels.

Methods

MD Simulation. All MD simulations were performed by using a constant temperature/constant axial pressure ensemble (5, 6). Periodic boundary conditions were applied only in the axial (z) direction. In the first, second, third, and fourth series of MD simulations, the simulation supercell contained 252, 300, 340, and 400 water molecules, respectively. The TIP5P water model (30) was used. The intermolecular interactions, including the long-range charge–charge interaction and the Lennard–Jones interaction between oxygen atoms, were truncated at 8.75 Å by a switching function (6). The potential function of the model single-walled CNTs (infinitely long) was taken to be a Lennard–Jones potential integrated over the cylindrical area of the CNT using the area density of the carbon atoms and the potential parameters for graphite (5, 6).

Structural Analysis. Instantaneous configurations (snapshots) generated in the MD simulations were mapped onto corresponding potential-energy local-minimum configurations using the constant-volume steepest-descent method. Some of the local-minimum configurations are shown in Figs. 1–4. In Fig. 5 [supporting information (SI) published online; not shown in the print edition], we also display a snapshot of double-walled helical ice at 250 K to compare with the corresponding local-minimum structures shown in Fig. 1 *a* and *b*.

Abbreviations: CNT, carbon nanotube; INT, ice nanotube; MD, molecular dynamics.

Author contributions: J.B. and X.C.Z. designed research; J.B., J.W., and X.C.Z. performed research; J.B., J.W., and X.C.Z. analyzed data; and X.C.Z. wrote the paper.

Acknowledgements

We thank Professors H. Tanaka, K. Koga, and P. Dussault for valuable discussions. This work was supported by Department of Energy Grant DE-FG02-04ER46164, the National Science Foundation (Divisions of Chemistry and Design and Manufacturing Innovation), the Nebraska Research Initiative, the John Simon Guggenheim Foundation, the National Science Foundation of China, and the Research Computing Facility at the University of Nebraska.

References

1. Lobban, C, Finney, JL & Kuhs, WF. (1998) *Nature* **391**, 268–270.
2. Salzmann, CG, Radaelli, PG, Hallbrucker, A, Mayer, E & Finney, JL. (2006) *Science* **311**, 1758–1761.
3. Kubo, T, Durham, WB, Stern, LA & Kirby, SH. (2006) *Science* **311**, 1267–1269.
4. Dore, J. (2000) *Chem Phys* **258**, 327–347.
5. Koga, K, Gao, GT, Tanaka, H & Zeng, XC. (2001) *Nature* **412**, 802–805.
6. Koga, K, Gao, GT, Tanaka, H & Zeng, XC. (2002) *Physica A* **314**, 462–469.
7. Maniwa, Y, Kataura, H, Abe, M, Suzuki, S, Achiba, Y, Kira, H & Matsuda, K. (2002) *J Phys Soc Jpn* **71**, 2863–2866.
8. Noon, WH, Ausman, KD, Smalley, RE & Ma, J. (2002) *Chem Phys Lett* **355**, 445–448.
9. Bai, J, Su, C-R, Parra, RD, Zeng, XC, Tanaka, H, Koga, K & Li, J-M. (2003) *J Chem Phys* **118**, 3913–3916.
10. Hung, FR, Dudziak, G, Sliwinska-Bartkowiak, M & Gubbins, KE. (2004) *Mol Phys* **102**, 223–234.
11. Ghosh, S, Ramanathan, KV & Sood, AK. (2004) *Europhys Lett* **65**, 678–684.
12. Kolesnikov, AI, Zanotti, J-M, Loong, CK, Thyagarajan, P, Morsvsky, AP, Loutfy, RO & Burnham, CJ. (2004) *Phys Rev Lett* **93**, 035503-1-4.
13. Maniwa, Y, Kataura, H, Abe, M, Udaka, A, Suzuki, S, Achiba, Y, Kira, H, Matsuda, K, Kadowaki, H & Okabe, Y. (2005) *Chem Phys Lett* **401**, 534–538.
14. Byl, O, Liu, JC, Wang, Y, Yim, WL, Johnson, JK & Yates, JT Jr. (2006) *J Am Chem Soc* **128**, 12090–12097.
15. Iijima, S. (1991) *Nature* **354**, 56–58.
16. Hummer, G, Rasaiah, JC & Noworyta, JP. (2001) *Nature* **414**, 188–191.
17. Maibaum, L & Chandler, D. (2003) *J Phys Chem B* **107**, 1189–1194.
18. Andreev, S, Reichman, D & Hummer, G. (2005) *J Chem Phys* **123**, 194502.
19. Marti, J & Gordillo, MC. (2001) *Phys Rev E* **64**, 165430.
20. Mann, DJ & Halls, MD. (2003) *Phys Rev Lett* **90**, 195503.
21. Mashl, JR, Joseph, S, Aluru, NR & Jakobsson, E. (2003) *Nano Lett* **3**, 589–592.
22. Naguib, N, Ye, H, Gogotsi, Y, Yazicioglu, AG, Megaridis, CM & Yoshimura, M. (2004) *Nano Lett* **4**, 2237–2243.
23. Wang, J, Zhu, Y, Zhou, J & Lu, X-H. (2004) *Phys Chem Chem Phys* **6**, 829–835.
24. Sriraman, S, Kevrekidis, IG & Hummer, G. (2005) *Phys Rev Lett* **95**, 130603.
25. Mamontov, E, Burnham, CJ, Chen, S-H, Moravsky, AP, Loong, C-K, de Souza, NR & Kolesnikov, AI. (2006) *J Chem Phys* **124**, 194703.
26. Petrenko, VF & Whitworth, RW. (1999) Physics of Ice (Oxford Univ Press, New York,).
27. Watson, JD & Crick, FHC. (1953) *Nature* **171**, 737.
28. Pauling, L. (1935) *J Am Chem Soc* **57**, 2680–2682.
29. Koga, K, Tanaka, H & Zeng, XC. (1997) *Phys Rev Lett* **79**, 5264–5267.
30. Mahoney, MW & Jorgensen, WL. (2000) *J Chem Phys* **112**, 8910–8922.

***Corresponding author:** email – xczeng@phase2.unl.edu

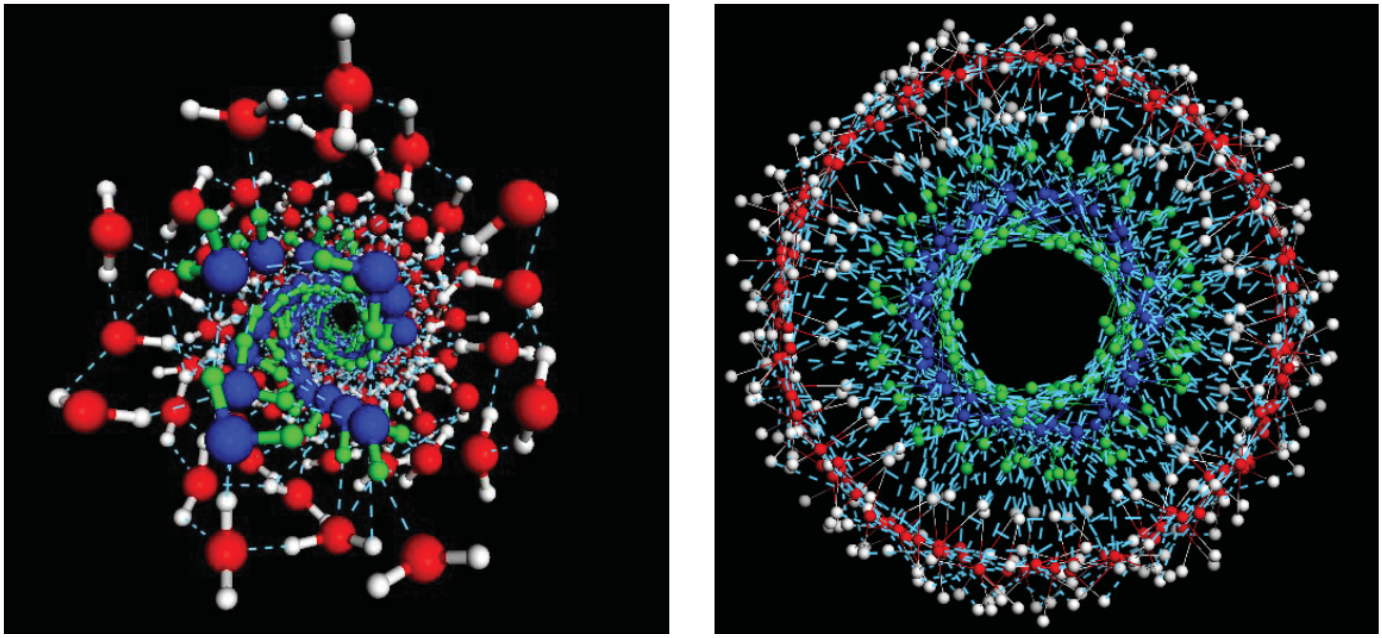

Fig. 5. Snapshots of the helical nanoice formed in (17,0) CNT at 4 GPa axial pressure and 250 K temperature. (*a*) Top view of the double-walled nano-ice helix in the axial direction where water molecules of the outer wall are in the red-white color while those of the inner wall are in the blue-green color (the blue dashed-lines denote hydrogen bonds). (*b*) Projected top-view in the axial direction. [This supporting information presented online at http://www.pnas.org/cgi/content/full/0608401104/DC1]